Materials Chemistry and Physics 270 (2021) 124852

Contents lists available at ScienceDirect

Materials Chemistry and Physics

journal homepage: www.elsevier.com/locate/matchemphys

Bioinspired aligned magnetic features in aerogels for humidity sensing

Josh Alexander [a], Karthikeyan Baskaran [b], Allison Harward [c], Krista Carlson [b], Steven E. Naleway [a,*]

[a] Department of Mechanical Engineering, University of Utah, 201 Presidents' Circle, Salt Lake City, UT 84112, USA
[b] Department of Materials Science and Engineering, University of Utah, 201 Presidents' Circle, Salt Lake City, UT 84112, USA
[c] Department of Chemical Engineering, University of Utah, 201 Presidents' Circle, Salt Lake City, UT 84112, USA

HIGHLIGHTS

- Ferrofluid forms aligned features in aerogels with applied magnetic fields.
- The volume of ferrofluid and applied field control the feature shape and size.
- Aligned features lead to increased magnetic susceptibility.
- Tunable aligned features can be used to control humidity responses.
- Aerogels with aligned features could be useful as specialized humidity sensors.

ARTICLE INFO

Keywords:
Aerogel
Magnetic alignment
Humidity sensing
Bioinspired

ABSTRACT

Many natural plant tissues, such as pinecones, utilize structures to transduce changes in humidity into movement or strain. These often employ layered structures with aligned features in order to create differential stress across the material as different portions swell at different rates. By replicating these types of structures in synthetic materials we can create structures that respond to humidity in a similar manner. Taking these aligned features as inspiration, silica aerogels with tailored humidity reactive properties were created. This behavior was achieved by creating aligned features in these aerogels using a Helmholtz coil to produce a uniform magnetic field that aligned ferrofluid droplets into chains and needle like features. These magnetite-based structures were shown to retain their superparamagnetic properties, allowing them to easily be removed from the aerogels, leaving a large number of aligned channels. Aerogels with the removed needles experienced significantly different strains than both unmodified aerogels and aerogels with the aligned features still in place. Aerogels with these tunable aligned features could be used in humidity sensors that can transduce changes in humidity into strain and could be used in applications such as volatile organic compound capture.

1. Introduction

Bioinspired design takes inspiration from the impressive structures found in biology to produce novel and useful synthetic materials and products. Examples include tape inspired by the hairs on gecko feet [1], superhydrophobic surfaces inspired by the surface of lotus leaves [2], and energy absorbing composites inspired by antlers and horns [3]. While bioinspired structures have been applied in a large variety of materials, they have yet to be used with aerogels to create structures that produce changes in shape from changes in humidity. These structures could allow for multifunctional aerogels that not only sense changes in humidity but can still maintain their utility for applications such as environmental air filtration [4,5] where harmful chemicals like formaldehyde can release at rates dependent on the relative humidity [6].

In nature, structures that are reactive to humidity give organisms unique advantages for survival. To ensure seeds are released at the right time, several species of plants have adapted methods to react to humidity [7]. An example from pinecones [8] is shown in Fig. 1 and other examples include Acanthaceae seeds [9] and wheat awn [10]. For each of these organisms the release mechanism is built passively into the structure holding the seed. For pinecones, this passive structure is dependent on two distinct layers of aligned, linear features formed from

* Corresponding author.
E-mail address: steven.naleway@mech.utah.edu (S.E. Naleway).

https://doi.org/10.1016/j.matchemphys.2021.124852
Received 25 March 2021; Received in revised form 24 May 2021; Accepted 15 June 2021
Available online 18 June 2021
0254-0584/© 2021 Elsevier B.V. All rights reserved.

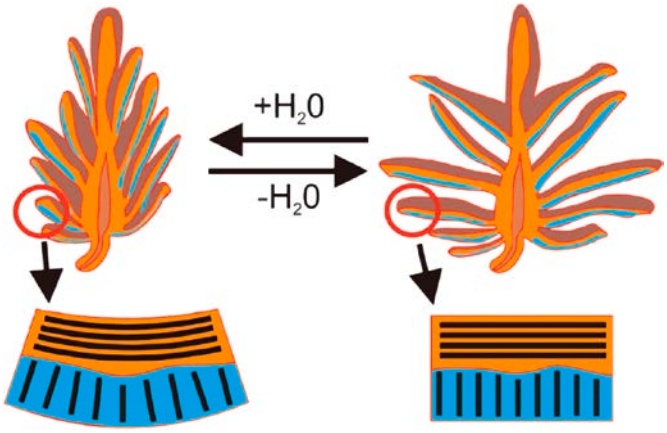

Fig. 1. Pinecones use aligned structures to react to humidity for effective seed dispersal. These aligned structures swell at different rates within the overall material leading to a bending motion that reveals the seeds inside. Figures adapted with permission from [15].

fibers and reacts to humidity similarly to how a bimetal strip reacts to a change in temperature (Fig. 1). One layer expands in a single direction while the other layer holds at a constant length leading to a bending motion that causes the pinecone's scale to open and reveal the seeds inside. The self-shaping strategies pinecones and other similar structures employ has led to many bioinspired materials ranging from ratcheting actuators for robotics [11] to flexible graphite-like humidity sensors [12]. In many cases, these bioinspired materials use magnetic particles and applied fields in order to control the orientation of structures inside the material [13,14].

This magnetic control stems from the ferromagnetic and superparamagnetic particles within the material. Ferromagnetic properties are quantum effects from the aligned spin of electrons [16]. Ferromagnetic materials like magnetite (Fe_3O_4) are composed of multiple magnetic domains where each domain consists of many atoms with aligned magnetic moments [17]. These domains can be aligned with an external magnetic field, which leads the bulk ferromagnetic material to react to the magnetic field. Superparamagnetic materials are small particles of ferromagnetic materials, such as magnetite, whose particle size is comparable to a that of a single ferromagnetic domain. They behave similarly to both ferromagnetic materials as they have high magnetic susceptibility however they have very low retentivity [18] unlike most ferromagnetic materials. These superparamagnetic particles only have one magnetic domain which can easily be reoriented in the absence of an external magnetic field due to thermal motion. For magnetite, as was employed in this research, this particle size threshold to act superparamagnetically is 30 nm [17].

One common use for these superparamagnetic materials is in ferrofluid, which is employed in applications like dynamic sealing, heat dissipation, and viscous damping [19]. Ferrofluid is made up of superparamagnetic particles coated in a surfactant that is distributed in a carrier fluid. These single domain magnetic particles remain distributed due to Brownian motion and have sizes ranging from 3 to 15 nm [20]. Due to the superparamagnetic properties of the suspended particles, ferrofluids are extremely magnetically susceptible to external magnetic fields and align or move towards the strongest areas of the field [19]. Due to this magnetic susceptibility, ferrofluid has been studied for many possible applications, including valves in microfluid systems [21], magnetically actuated surfaces with low friction [22], and for creating field-controlled microneedle molds [14], to name a few.

To harness ferrofluids in bulk and bioinspired materials, they must be incorporated into a matrix. One such matrix material that has proven promising is aerogels. Aerogels are materials made by removing the liquid from gels, such as hydrogels or alcogels. These hydrogels and alcogels are crosslinked networks with water or alcohol, respectively, filling the remaining space [23]. Supercritical drying is typically used to remove these liquids to form aerogels, as this process enables the removal of the liquid with minimal structural collapse because it eliminates the forces that arise from capillary action when drying under ambient pressure [24]. This drying leaves behind the porous network that makes up the aerogel. The porous network provides aerogels with many desirable properties, such as extremely low densities, high strength to weight ratios, and high surface areas [25]. Aerogels have been made from many inorganic and organic materials, such as silica [26], graphene [27], or cellulose [28]. These properties allow aerogels to be successful in a number of applications including thermal and acoustic insulation [29], high velocity particle capture [30], catalysts and catalyst support [31], and filters [32].

One emerging possible application for aerogels is in humidity sensing. Sensors for detecting changes in humidity have been developed with a wide variety of materials, ranging from paper [33], SnS_2/Zn_2SnO_4 films [34], to silica [35] or gold-based aerogels [36]. Silica aerogels, a commonly researched type of aerogel, have been used for transducing changes in humidity into changes in impedance and capacitance [35]. More recently gold aerogels were used to create highly sensitive structures that responded to humidity changes from human breath [36]. The success of these silica and gold aerogels was linked to the high porosity and surface area provided by the structure of the aerogel's network. These aerogels can be made using a silicon alkoxide, such as tetraethyl orthosilicate (TEOS), which allows for easy fabrication of silica aerogels. When TEOS in alcohol is reacted with water and a base catalyst, silica nanoparticles form that, in turn,aggregate and bond to form the network of an alcogel.

Aerogel applications have also begun to expand through the incorporation of magnetic components. To date, magnetic particles have been introduced to aerogels to create materials for medical hyperthermia applications [37], EMI shielding, and as drug delivery agents [38]. In addition to altering the properties of these aerogels, magnetic particles also allow for control of the structure by using applied magnetic fields during formation. By controlling the orientation of cobalt nanorods, ultralight magnets with magnetic anisotropy were created [39]. By applying a strong magnetic field of 1 T to dispersed magnetite particles, templates for silica deposition were formed that led to a large change in the size and shape of pores within the produced aerogel [40]. Similar techniques have also been used in titania and anatase aerogels to create layered structures [41]. Similar needle like structures have also been created by using larger particles of iron powder in silica aerogels by using magnetic fields up to 4.6 T [42]. One disadvantage of all of these methods is that they require permanent magnets or extremely strong applied fields greater than 1 T to form features. To date, there has yet to be a method to employ aerogels and magnetic particles for bioinspired structures as humidity-responsive materials using low-strength ($<$1 T) magnetic fields.

This work investigates a new method for creating magnetically aligned features for humidity response inspired by the aligned features in pinecones. The magnetic fields used to create these features are significantly weaker ($\approx$0.01 T) than those used in previous work [40,42] and used the uniform field of a Helmholtz coil to produce uniform features across the aerogel. In addition, the unique shape of the features within these aerogels were influenced by the use of ferrofluid during gelation rather than individual particles dispersed directly in the precursors. The features created by this magnetic alignment exhibited much stronger magnetic susceptibility than randomly distributed particles allowing for their easy removal from the aerogels, which resulted in aligned channels. Aerogels with these aligned channels mimic the structure of pinecones and responded in a significantly different manner to humidity when compared to both unmodified aerogels as well as aerogels with magnetically aligned features. The strain created in these aligned channel aerogels in response to humidity makes them ideal for applications where a reaction to humidity is required, such as when

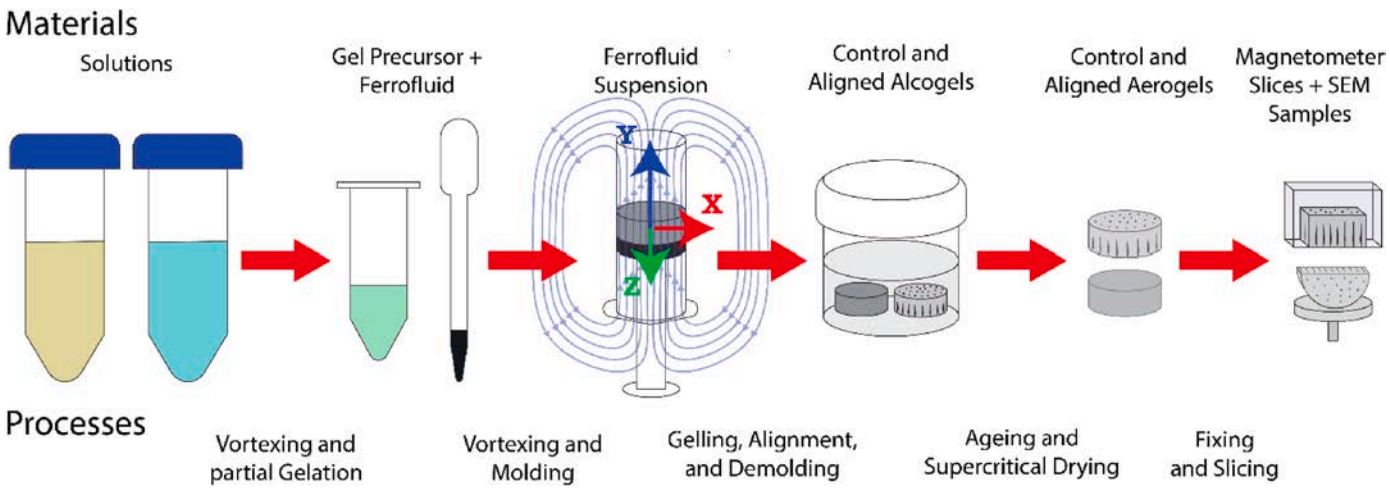

Fig. 2. The process for creating magnetically aligned aerogels begins with two solutions being vortexed. This mixture gels around ferrofluid droplets which can be aligned by applying magnetic fields. Supercritical drying turns the produced alcogels into aerogels which can then be processed for testing.

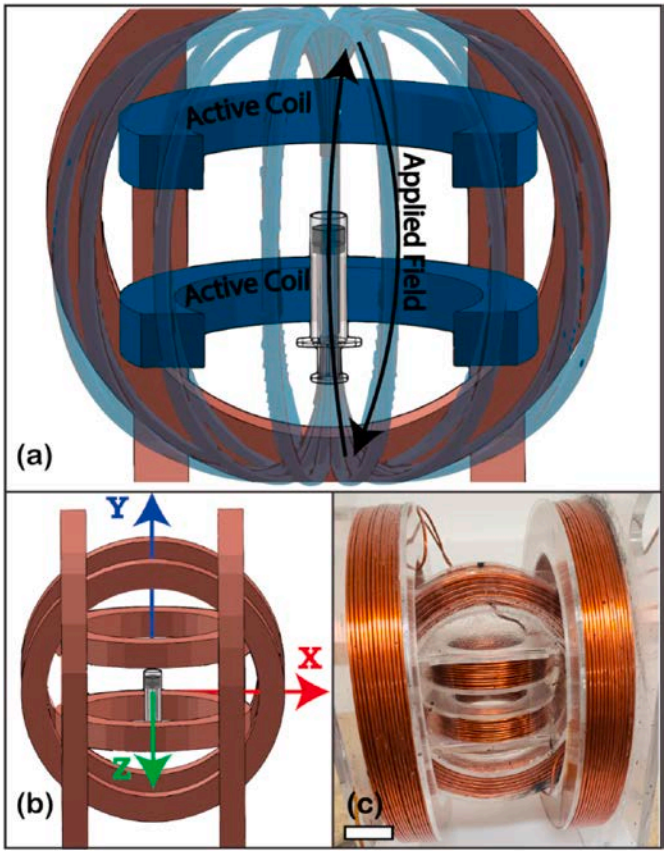

Fig. 3. The triaxial Helmholtz coil used to apply a magnetic field during gelation can generate a magnetic field in any direction depending on which coil is active. Note that in this research, only the smallest set of coils were employed to create a magnetic field in the y direction. (a) The magnetic field shown in blue was applied along the y axis by using the two smallest coils. (b) When run alone, each pair of coils generates a uniform magnetic field around the syringe along the axes shown. (c) The triaxial Helmholtz coil used for this study can generate magnetic fields up to 10 mT, in any direction. The scale bar is 5 cm. (For interpretation of the references to colour in this figure legend, the reader is referred to the Web version of this article.)

dealing with volatile organic compounds (VOC) whose release rates can depend on humidity.

2. Materials and methods

2.1. Magnetically aligned aerogels

Fig. 2 shows the process used to form the control aerogels and aerogels with magnetically aligned features. Alcogels were prepared using a sol-gel process from two solutions as used in previous work [43]. The first solution was made with 57.895 v% 200 proof ethanol (Decon Labs, Philadelphia, PA, USA) and 42.105 v% tetraethyl ortho-silicate (TEOS) (Sigma-Aldrich, St. Louis, MO, USA). The second solution contained 76.923 v% 200 proof ethanol, 20.979 v% deionized water and 2.098 v% catalyst. The catalyst was composed of 18.278 v% ammonium hydroxide (Reagent Grade, Pfaltz &Bauer, Waterbury, CT, USA) and 1.486 v% ammonium fluoride (96%, Alfa Aesar, Ward Hill, MA, USA) with the remainder being deionized water. One mL of gel precursor was prepared by mixing 63.86 v% of the first solution with 36.14 v% of the second solution using a vortex mixer. The precursor was vortexed for 1 min and then allowed to stand for the hydrolysis and condensation reactions to begin. Note that the total volume of the gel precursor was always maintained at one mL. Ferrofluid (EFH1 fluid, Ferrotec, Santa Clara, CA, USA) was added when two thirds of the expected gel time had passed and then vortexed for 15 s. Expected gel time was determined experimentally for each batch of solutions and usually was around 4 min $\pm$ 2 min. Ferrofluid was added in amounts to make ferrofluid suspensions of ten, fifteen, and twenty v% ferrofluid. The ferrofluid added used a hydrocarbon as its carrier fluid, leading to hydrophobic interactions with the ethanol. This ferrofluid suspension was then poured into a syringe, which was used as a mold, and capped with parafilm. The ferrofluid suspension was then allowed to gel for 15 min.

Alcogels with magnetically aligned structures were created using a 10 mT applied magnetic field. This magnetic field was applied along the y direction as shown in Fig. 3 during the 15 min of gel time. The field was applied using a Helmholtz coil as described in previous work [44]. A Helmholtz coil was chosen as the volume at the center of the coil experiences a very uniform magnetic field such that a field gradient does not develop and cause magnetic particles to agglomerate.

After 15 min the alcogels were removed from the molds and placed into 200 proof ethanol to age and wash any remaining water, ferrofluid surfactant, or carrier fluid from the alcogels. The ethanol was changed twice at a minimum of 24 h apart. 24 h after the last fluid exchange the alcogels were dried in a super critical drier (CDPD2 2400, Ted Pella,

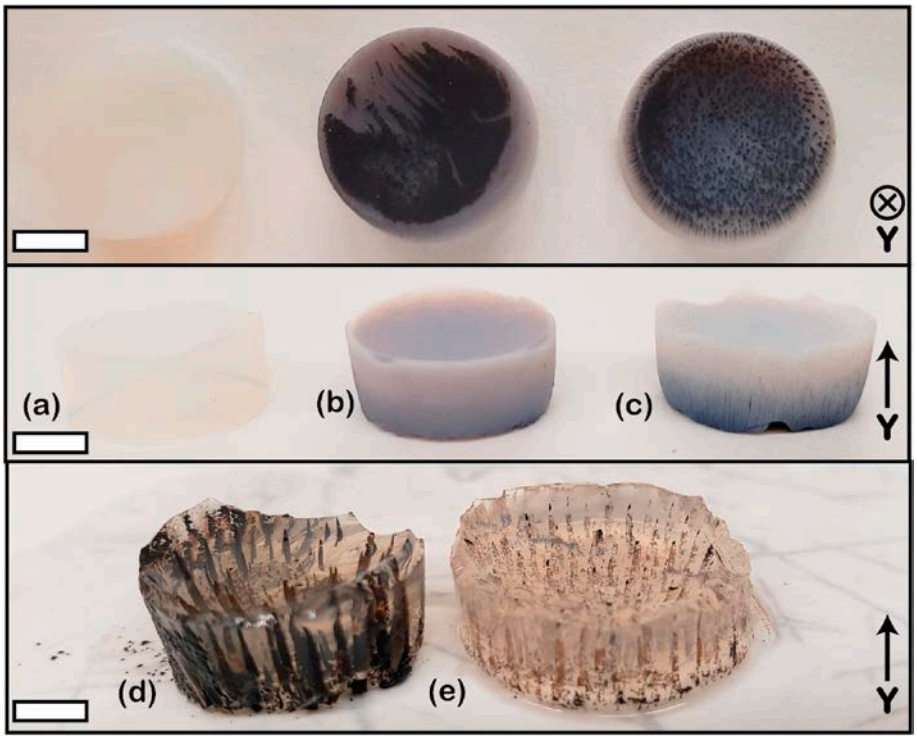

Fig. 4. Examples of (a) unmodified silica aerogels, (b) control aerogels with magnetite particles, and (c) aerogels with magnetically aligned features that are visible to the naked eye. By simply holding a magnet below (d) alcogels with magnetically aligned features, the needle like features can easily be removed to produce (e) aerogels with aligned channels. Note the aerogels (b) and (c) were made with ten v% ferrofluid and the alcogels (d) and (e) with twenty v%. Scale bars are 3 mm for the aerogels (a)–(c) and 4 mm for the alcogels (d)–(e). Note the aerogel samples shown in the top row are the same samples as those directly below them.

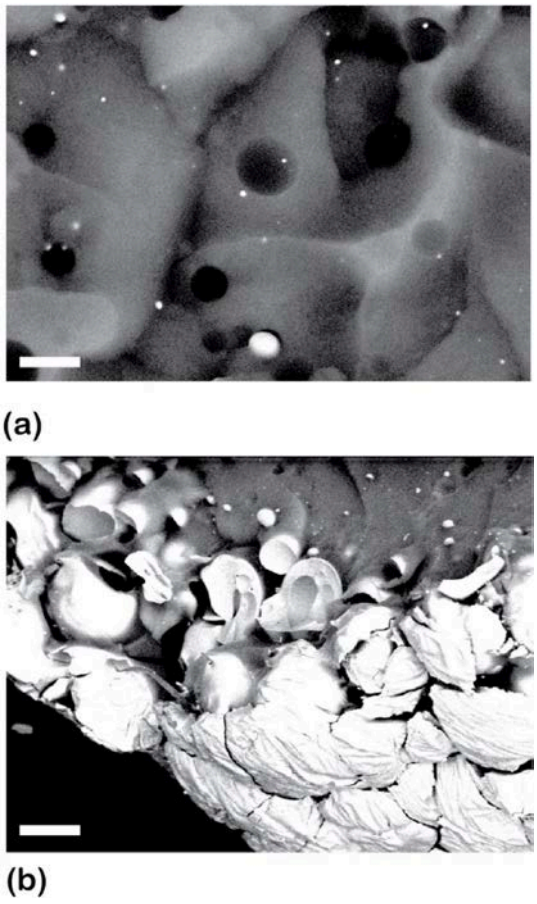

Fig. 5. The magnetite-based particles (shown in white) within the control aerogels (a) dispersed in control aerogels, which also settled towards the bottom of the gel during gelation to produce a (b) magnetite heavy crust with spherical particles formed from ferrofluid droplets. Scale bars are 150 μm.

Redding, CA, USA) using carbon dioxide to produce aerogels. For aerogels undergoing humidity testing, the initial ethanol used for the solvent exchange was replaced with a mixture of 50 v% ethanol 50 v% dimethyldiethoxysilane (DMDES, Sigma-Aldrich, St. Louis, MO, USA) to add hydrophobic CH_3 end groups over the surface of the pores in the resultant aerogels without altering their microstructure. The addition of CH_3 end groups ensured minimal structural damage during adsorption and desorption of water. The aerogels were cylindrical in shape with a diameter of 11–13 mm and height of 3.3–4.5 mm and were predominately silica with iron-oxide inclusions that, in the case of aligned aerogels, formed magnetically aligned features, as shown in Fig. 4. A total of eighteen aligned aerogels were made for imaging and magnetic property testing, six of each ferrofluid v%. In addition, six control aerogels of each ferrofluid v% were made without an applied magnetic field for same purposes. Twenty-eight total aerogels were made for hydration testing. Seven of these were made without any added ferrofluid or applied field, the remaining twenty-one were made with twenty mL of ferrofluid: seven with no applied field, seven with magnetically aligned features from an applied 10 mT field, and seven where these features were removed prior to ageing using a permanent magnet.

2.2. Aerogel characterization and imaging

Aerogels were imaged using a scanning electron microscope (SEM, FEI Quanta 600 FEG, FEI, Hillsboro, OR, USA). Three aligned aerogels and three controls at each v% were used for characterization. To prepare samples for the SEM, aerogels were cut in half perpendicular to the x-z plane of the aerogel and then bonded to an aluminum stub using carbon tape with the cut side facing up. Energy dispersive X-ray spectroscopy (EDS) was used to confirm the chemical composition of the aerogels and to determine the location of iron within the aerogels.

To obtain counts and sizes of the magnetically aligned features the back-scatter detector was used to highlight the iron-based features. For this an accelerating voltage of 20 kV and spot size of 5 nm was used. These images were stitched together using ImageJ. Measurements of every aligned feature was made using ImageJ for three full aerogel images of each ferrofluid concentration and type of applied field. All

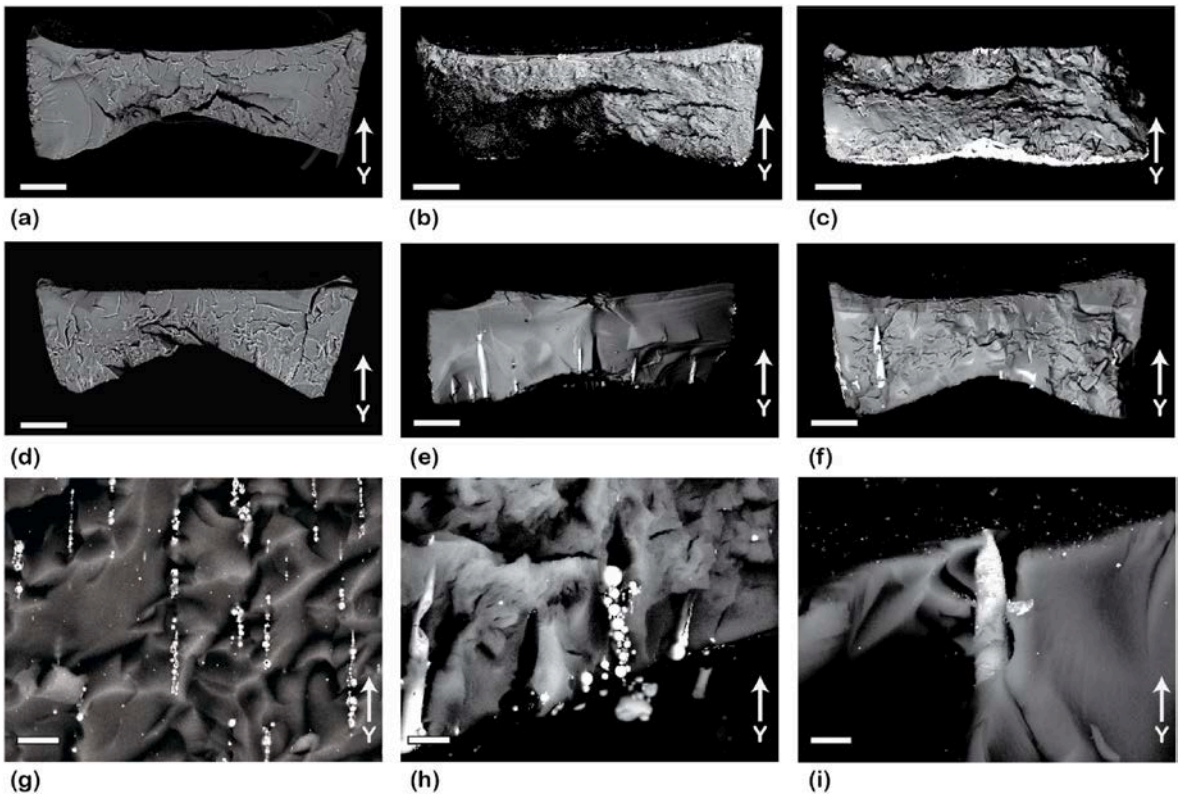

Fig. 6. x-y cross sections of the aerogels and feature highlights. For (a), (b), (c) control aerogels as the v% of ferrofluid increased from (a) ten to (b) fifteen to (c) twenty. The main change that can be seen is a thicker magnetite crust along the bottom of the aerogel. For (d), (e), (f) magnetically aligned aerogels as the v% increased from (d) ten to (e) fifteen to (f) twenty, the type and distribution of the features changed. At higher magnification at 10 v% (g) chains of droplet features were apparent, which began to be replaced with some continuous needle like features at 15 v% (h). As the v% further increased to 20 v% (i) much larger needle like features were observed. Scale bars are 2 mm for (a)–(f) and 100 μm for (g)–(i).

aligned feature lengths were recorded along with their width and angle relative to the x-z plane of the Helmholtz coil setup. These properties were measured by drawing lines in ImageJ along the feature's length and across its widest section. Features below 0.1 mm in length were ignored as their angles were subject to more variability due to the size of the pixels in the digital images. For the features that were chains of droplet-based spheres the width of the largest single sphere was measured and considered to be the width of the feature. In addition to overall images, images of the microstructure of the aerogel were taken using a much smaller accelerating voltage of 2 kV with a spot size of 2 nm as the silica structure was prone to charging. In total 296 feature widths and heights were measured. For the characterization of the aligned magnetic features the number of features varied by v% with ten, fifteen, and twenty percent having 271, 17, and 8 measured features, respectively. None of the control aerogels displayed any aligned features so no direct comparisons were made.

2.3. Magnetic property testing

Three aligned aerogels and three control aerogels at each ferrofluid v % were used for magnetic testing. Aerogels were prepared for magnetic characterization by first mounting them in two-part epoxy (Epoxicure 2, Buehler, Lake Bluff, IL, USA). Two slices of each epoxy mounted sample were cut out using a low-speed diamond saw to a size of approximately 7 mm × 7 mm × 2 mm. These slices were then weighed using a scale. The magnetic susceptibility was then found from generated hysteresis curves using a vibrating sample magnetometer (MicroSense FCM-10, KLA, Milpitas, CA, USA). Magnetic measurements were made on the six slices for each of the v% for both the control aerogels as well as the aerogels formed under an applied magnetic field. The magnetic susceptibility was then divided by the weight of the slice to determine the mass magnetization. The susceptibility was then compared between aerogels with and without magnetically aligned features to determine the effect of particle alignment on magnetic susceptibility.

2.4. Humidity testing

Twenty-eight total aerogels were placed into a vacuum chamber for 24 h prior to being placed into a humidity chamber (TE-101 H–F, Test Equity LLC Moorpark, CA). Seven of these were plain aerogels without any added ferrofluid or applied field, the remaining twenty-one were made with twenty v% ferrofluid: seven with no applied field, seven with magnetically aligned features from an applied 10 mT field, and seven where these features were removed using a permanent magnet. Aerogels with twenty v% were used as they formed the largest features, which proved to be the easiest to remove. Four aerogels of each type were placed into a humidity chamber at 90% humidity for 24 h. The remaining aerogels were placed into the same chamber at 45% humidity, also for 24 h. The aerogels thickness and diameter were recorded prior to being placed into the chamber and then again immediately after being removed. The strain was then calculated for both diameter and thickness and compared between aerogel types. To investigate the desorption and repeatability of the aerogel humidity response, the aerogels that were placed into 90% humidity were retested and placed back into the vacuum chamber for 24 h, followed by 24 h at 90% humidity in the humidity chamber.

2.5. Statistical analysis

The height, width, magnetic susceptibility, strain across the diameter after hydration, and strain across the thickness after hydration were compared between v% and magnetic conditions using a one-way

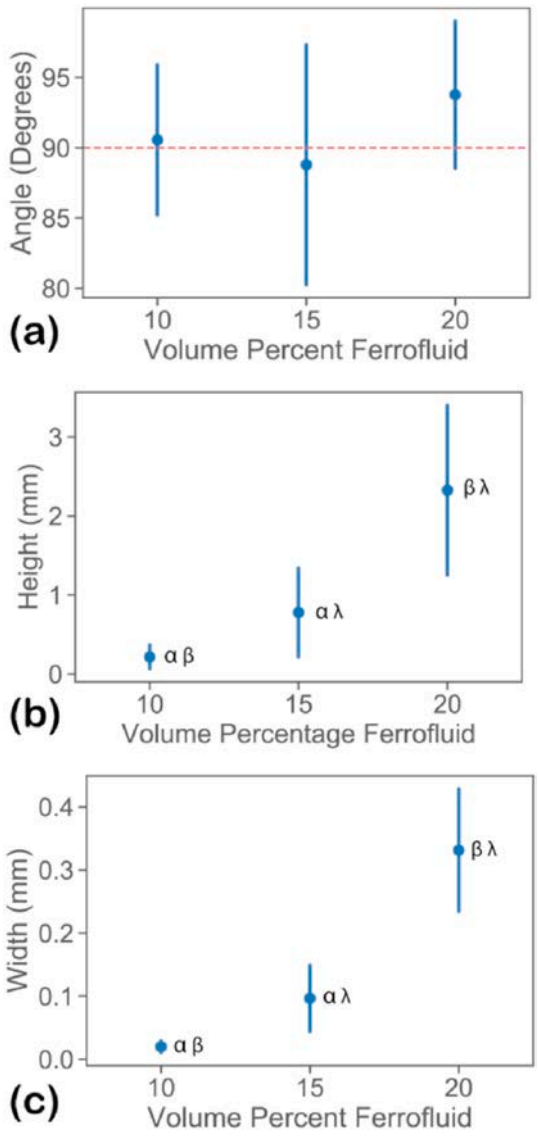

Fig. 7. Plots displaying the (a) angle from the applied magnetic field, (b) feature height, and (c) feature width of the magnetically aligned features as a function of v% of ferrofluid. Data is presented with error bars representing the mean ± one standard deviation with each data point at ten, fifteen, and twenty v% representing 271, 17, and 8 measurements, respectively. Statistically significant differences between pairs of groups are represented by matching Greek letters next to each group's mean.

ANOVA. If a statistically significant difference was found a Tukey HSD test was run to find significant differences between groups. For the feature angle measurements a one-mean *t*-test was used to find any relevant statistical significance. All calculations and analysis were performed in Python using the SciPy and stats models libraries. The confidence level used for these tests was 0.95 meaning a p-value of less than 0.05 in a comparison was considered to show statistically significant results. In all graphs, statistically significant differences between pairs of groups is denoted by a matching Greek letters placed next to the mean of each of the two groups.

3. Results and discussion

When ferrofluid was mixed into an alcogel during the gelling process without an applied magnetic field, the resulting aerogel displayed a variety of structures depending on the v% ferrofluid and magnetic field applied during gelling. Fig. 5 shows two common features in the control composite aerogels with no applied magnetic field. A typical distribution of droplets is shown Fig. 5a. These droplets were distributed throughout the aerogel and were usually spherical with a diameter on the order of micrometers to tens of micrometers. These spheres were formed from the suspended ferrofluid droplets that were distributed during vortexing and remained separate due to hydrophobic interactions. In addition, these control aerogels also had an iron heavy crust along the bottom of the aerogel, as shown in Fig. 5b. This crust was more prevalent among aerogels with higher v% ferrofluid, as seen in Fig. 6a–c, where the increased volume of ferrofluid settled and combined due to its greater density.

When a magnetic field was applied to these distributed droplets, they aligned along the direction of the field to form varying types of magnetically aligned features (Fig. 6d–i) that were distributed across the aerogel. By using a Helmholtz coil to apply a magnetic field, the alignment of these features remained relatively consistent across the aerogel as shown Fig. 7a, as opposed agglomerating near the edges of the aerogels. For each of the v%, a one mean *t*-test revealed no statistically significant differences in angle from the applied field direction in the magnetic field, which was applied along the y axis ($p > 0.56$). This demonstrated that the uniform field produced by the Helmholtz coil effectively produced uniform aligned features parallel with the magnetic field. The size of these features varied as a function of the v% of ferrofluid as shown Fig. 7b–c. For both height and width all possible comparisons between v% showed significant differences ($p < 0.001$). As more ferrofluid was added, the size of the features increased from an average of 0.217 mm at ten percent volume ferrofluid to 0.779 mm at fifteen and then 2.328 mm at twenty. The width also increased from 0.0198 mm to 0.0964 mm and then to 0.331 mm as the v% increased from ten to fifteen to twenty. This increase in feature size coincided with a decrease in the number of features per aerogel leading to fewer but much larger features.

Not only did the magnetically aligned features change in size as more ferrofluid was added, but the shape of the features changed as well. Fig. 8 shows characteristic features with no applied mangetic field (a) and as the v% changes from ten to fifteen to twenty, along with EDS to demonstrate the composition of the features. At ten percent (Fig. 8b), the droplets formed vertical chains, indicating the structure was influenced by the magnetic properties of the superparamagnetic particles responding to the applied magnetic field. However, at this low v%, the particles did not touch and remained chains of individual droplets due to hydrophobic forces. The introduction of greater amounts of ferrofluid allowed the associated magnetic force to overcome these hydrophobic forces. As the percentage increased to fifteen (Fig. 8c) these droplets combined to form cone-like needle features. Chains of droplets remained within the fifteen percent aerogels and droplets could be observed. As the percentage further increased to twenty percent (Fig. 8d) the needles become both taller and wider. This produced an aerogel with fewer but much larger needles. These needles were either solid or hollow with a standard silica aerogel structure inside. As shown from the EDS imagery, the features were made from iron and oxygen, while the matrix was silicon and oxygen.

The addition of the ferrofluid to the aerogel produced a composite structure with magnetic properties. This composite material retained some of the magnetic characteristics of the added superparamagnetic particles from the ferrofluid. Fig. 9 shows the changes in magnetic properties caused by changing the volume of ferrofluid added and the magnetic field applied during formation of the aerogel. There was no statistically significant difference in magnetic saturation for the control aerogels, which contained non-aligned ferrofluid, as all of the aerogels were essentially not susceptible to the magnetic field. However, as soon as the particles were aligned into linear features significant differences began to appear. The clearest example of this was at twenty v% where the magnetic saturation of the free component went from an average of 0.113 emu/g to 2.11 emu/g for aerogels without a magnetic field and with the application of a 10 mT magnetic field, respectively. This type of

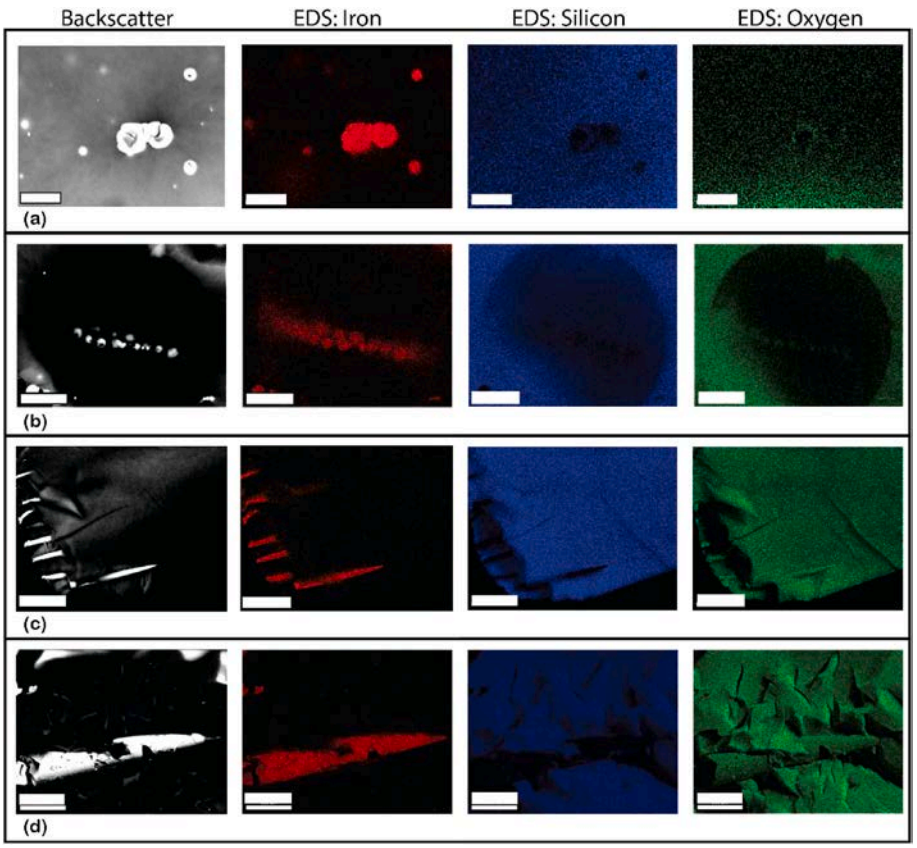

Fig. 8. Energy Dispersive X-ray Spectroscopy (EDS) images taken of common features within the aerogels. Images are shown as a group with a backscatter SEM image and the corresponding EDS images. (a) When no magnetic field is applied the iron based particles are distributed throughout the silica network. (b) When applying a magnetic field with 10 v% ferrofluid, the iron particles organize into chains of droplets. (c) When applying a magnetic field with 15 v% ferrofluid, iron needle features begin to appear. (d) When applying a magnetic field with 20 v% ferrofluid, these needles get significantly larger. Scale bars are 20 μm for (a), 50 μm for (b), and 500 μm for (c)–(d). Oxygen can be found in all of these iron based features demonstrating that the material is iron oxide. However, there are gaps in the silicon where the iron is present, demonstrating that the iron has been segregated from the silica matrix. (For interpretation of the references to colour in this figure legend, the reader is referred to the Web version of this article.)

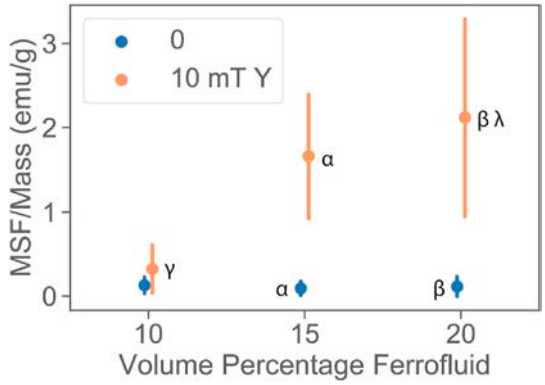

Fig. 9. Plot displaying the magnetic saturation of the free components (MSF). There is no difference, and essentially no magnetic susceptibility, across v% ferrofluid for control aerogels formed without an applied magnetic field. The magnetic saturation of the free component increased by factors greater than 10 at both fifteen and twenty v% ferrofluid ($p < 0.01$). Data is presented with error bars representing the mean ± one standard deviation with each data point representing six measurements across three samples. Statistically significant differences between pairs of groups are represented by matching Greek letters next to each group's mean.

statistically significant increase was seen at both fifteen and twenty v% with associated p values all being below 0.01 when compared to ten v%. In addition to differences caused by magnetic alignment there was also significant increases associated with the addition of more ferrofluid. The magnetic saturation of the free component increased from 0.321 emu/g to 2.12 emu/g. As a result of the higher magnetic susceptibility of these magnetically aligned features, permanent magnets could easily be used to physically separate and remove them. This allowed the creation of aerogels with multiscale porosity with controllably aligned channels, as shown in Fig. 4d–e. Focus was placed on creating aerogels with removed channels from aerogels made with twenty v% ferrofluid. The larger features in these aerogels and their increased magnetic susceptibility led to easier feature removal and subsequently more crack free aerogels when compared to the ten and fifteen v% aerogels.

In addition to increasing the magnetic susceptibility of the aerogel, these aligned structures also impacted the way these aerogels swell under changing humidity. As has been shown in previous work [45], condensation of water on the silica network will not occur until 60% humidity at room temperature. Past this critical point capillary condensation occurs and liquid water condenses in the network. This condensed moisture causes bridging between the silica particles as the water reacts with the Si–OH end groups to form Si–O–Si, which can break down back to Si–OH leading to dimensional changes in the gel [46]. For the aerogels placed in 45% humidity this was confirmed by a lack of any significant change in either diameter or thickness. However, as the humidity was changed to 90%, well past this 60% threshold, significant changes in the macrostructure were observed. As shown in Fig. 10a, the strains developed along the diameter of aerogels when in a high humidity environment was significantly larger for aerogels with linear aligned features (needles) and aerogels with linear features that had been removed (removed) than for unmodified aerogels with no added ferrofluid (plain) ($p < 0.02$). Both the aerogels with linear aligned features and those where these features were removed had engineering strains that were at least 49% larger than those for the aerogels with no added ferrofluid. However, these aligned features restrained the aerogels from changing in thickness (Fig. 10b). By removing these aligned features, the strain increased by more than 92% ($p < 0.015$) when compared to aerogels with the aligned features still present. These trends in the aerogel responses to humidity are due to the access of moisture to the pores inside the aerogel. Plain aerogels have an even distribution of pore structures leading to the limited movement of

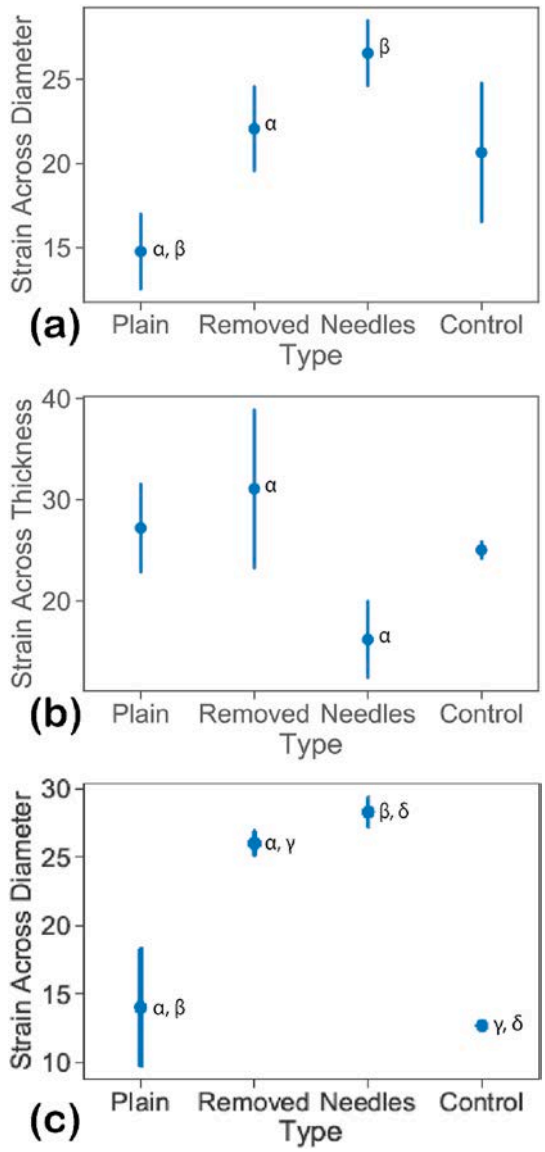

Fig. 10. Plots displaying the strain across the (a) diameter and (b) thickness after hydration at 90% humidity and (c) diameter after a second exposure to 90% humidity for aerogels formed under different conditions. Both the aerogels with removed aligned features (removed) and those with the needle-like aligned features (needles) change diameter by more than 49% when compared to silica aerogels with no added ferrofluid (plain). After a second exposure to 90% humidity the aerogels showed a very similar response across the diameter with significant differences still being shown between unmodified aerogels and those with aligned features. Data is presented with error bars representing the mean ± one standard deviation with each data point representing four samples. Statistically significant differences between pairs of groups are represented by matching Greek letters next to each group's mean.

condensed water. While control aerogels (control) have a similar pore structure, the presence of metal ferrofluid particles accelerates the nucleation of water, leading to more change than plain aerogels. Aerogels where the aligned features have been removed have a hierarchical pore structure where a large pore leads to smaller pores. This hierarchical pore structure provides increased access for moisture inside the aerogel, causing more pronounced deformation. Following the trend with plain and control aerogels, the presence of unremoved needle structures nucleate more water and can also cause capillary movement of condensed water, thus showing the highest deformation.

These aligned features also proved to continue to produce significantly different responses after a second cycle in vacuum and 90% humidity. After the aerogels were replaced in vacuum after exposure to 90% humidity some of their dimensions reversed, however significant differences were still observed from the initial measurements prior to any humidity treatments. Even though the aerogels did not fully recover, Fig. 10c shows that their reaction to a second exposure at 90% humidity produced similar humidity responses to their first exposure with similar levels of significance ($p < 0.015$). By using magnetic fields to create magnetically features and permanent magnets to remove these features for aligned channels, aerogels could be created with tailored responses to changes in humidity that show repeatable responses across multiple exposures.

Given their susceptibility to changes in humidity, aerogels with aligned channels offer an ideal solution for humidity sensing under complex circumstances where needs for repeatability, changes in sensitivity over a range of humidity, and environmental factors such as the presence of VOCs complicate the requirements for a sensor. Since they maintain all of the properties that make them useful for filtering and adsorption like high porosity and surface area, these materials could also be ideal for circumstances of automated environmental contaminant capture. This humidity-based swelling could be employed in a manner similar to how the pinecone reacts to humidity for seed dispersal.

4. Conclusions

Based on a study of modifying aerogels with added ferrofluid and uniform magnetic fields generated by a Helmholtz coil, it has been demonstrated that magnetically aligned features could be created that alter aerogel properties in the following ways.

- Applying uniform magnetic fields to aerogels with added ferrofluid during gelation results in aligned features that took the form of needle and droplet chain structures depending on the volume concentration of the ferrofluid.
- Aerogels with magnetically aligned features of magnetite were significantly more (18× to 40x) magnetically susceptible to external fields. This increased susceptibility allowed these aligned features to be removed from the aerogel after gelation using a permanent magnet.
- Aerogels with removed aligned features reacted to changes in humidity with strains across the diameter that were 49% larger than those for unmodified aerogels and strains across the thickness that were 92% larger than those for aerogels with aligned features. This allowed for structurally controlled humidity responses.
- Aerogels with modified physical humidity responses could be useful for sensors that also require other capabilities that aerogels are known for such as adsorption or filtration.

CRediT authorship contribution statement

Josh Alexander: Data curation, Conceptualization, Formal analysis, Writing – original draft. **Karthikeyan Baskaran:** Data curation, Writing – review & editing. **Allison Harward:** Data curation, Writing – review & editing. **Krista Carlson:** Conceptualization, Writing – review & editing. **Steven E. Naleway:** Project administration, Conceptualization, Writing – review & editing.

Declaration of competing interest

The authors declare that they have no known competing financial interests or personal relationships that could have appeared to influence the work reported in this paper.

Acknowledgements

Silica gel composition selection and hydration testing were support by the United States Department of Energy (DOE) Office of Nuclear Energy's Nuclear Energy University Programs (DE-NE0008900).

References

[1] L. Ge, S. Sethi, L. Ci, P.M. Ajayan, A. Dhinojwala, Carbon nanotube-based synthetic gecko tapes, Proc. Natl. Acad. Sci. Unit. States Am. 104 (26) (Jun. 2007) 10792–10795, https://doi.org/10.1073/pnas.0703505104.
[2] A. Neto, H. Meredith, C. Jenkins, J. Wilker, J.F. Mano, Combining biomimetic principles from the lotus leaf and mussel adhesive: polystyrene films with superhydrophobic and adhesive layers, RSC Adv. 3 (May 2013) 9352–9356, https://doi.org/10.1039/C3RA40715B.
[3] J. McKittrick, et al., Energy absorbent natural materials and bioinspired design strategies: a review, Mater. Sci. Eng. C 30 (3) (Apr. 2010) 331–342, https://doi.org/10.1016/j.msec.2010.01.011.
[4] C. Mustansar Hussain, A.K. Mishra, New Polymer Nanocomposites for Environmental Remediation, Elsevier, San Diego, UNITED STATES, 2018.
[5] H. Maleki, Recent advances in aerogels for environmental remediation applications: a review, Chem. Eng. J. 300 (Sep. 2016) 98–118, https://doi.org/10.1016/j.cej.2016.04.098.
[6] S. Zhou, H. Liu, Y. Ding, Y. Wu, The effects of temperature and humidity on the VOC emission rate from dry building materials, IOP Conf. Ser. Mater. Sci. Eng. 609 (Oct. 2019), 042001, https://doi.org/10.1088/1757-899X/609/4/042001.
[7] J.M. Losada, N. Blanco-Moure, A.B. Leslie, "Not all 'pine cones' flex: functional trade-offs and the evolution of seed release mechanisms, New Phytol. 222 (1) (2019) 396–407, https://doi.org/10.1111/nph.15563.
[8] C. Dawson, J.F.V. Vincent, A.-M. Rocca, How pine cones open, Nature 390 (Dec. 1997) 6661, https://doi.org/10.1038/37745. Art. no. 6661.
[9] A. Witztum, K. Schulgasser, The mechanics of seed expulsion in Acanthaceae, J. Theor. Biol. 176 (4) (Oct. 1995) 531–542, https://doi.org/10.1006/jtbi.1995.0219.
[10] R. Elbaum, L. Zaltzman, I. Burgert, P. Fratzl, The role of wheat awns in the seed dispersal unit, Science 316 (5826) (May 2007) 884–886, https://doi.org/10.1126/science.1140097.
[11] B. Shin, et al., Hygrobot: a self-locomotive ratcheted actuator powered by environmental humidity, Science Robot 3 (14) (Jan. 2018) eaar2629, https://doi.org/10.1126/scirobotics.aar2629.
[12] T. Nakajima, T. Nakamura, T. Tsuchiya, Flexible humidity sensors composed of graphite-like carbon micro-pinecone arrays, RSC Adv. 6 (97) (2016) 95342–95348, https://doi.org/10.1039/C6RA21902K.
[13] R.M. Erb, J.S. Sander, R. Grisch, A.R. Studart, Self-shaping composites with programmable bioinspired microstructures, Nat. Commun. 4 (1) (Apr. 2013), https://doi.org/10.1038/ncomms2666. Art. no. 1.
[14] X. Zhang, et al., Bio-inspired clamping microneedle arrays from flexible ferrofluid-configured moldings, Sci. Bull. 64 (15) (Aug. 2019) 1110–1117, https://doi.org/10.1016/j.scib.2019.06.016.
[15] J.W.C. Dunlop, R. Weinkamer, P. Fratzl, Artful interfaces within biological materials, Mater. Today 14 (3) (Mar. 2011) 70–78, https://doi.org/10.1016/S1369-7021(11)70056-6.
[16] H. Jin, T. Miyazaki, Basis of magnetism, in: T. Miyazaki, H. Jin (Eds.), The Physics Of Ferromagnetism, Springer, Berlin, Heidelberg, 2012, pp. 3–33, https://doi.org/10.1007/978-3-642-25583-0_1.
[17] D.J. Dunlop, Superparamagnetic and single-domain threshold sizes in magnetite, J. Geophys. Res. 78 (11) (1973) 1780–1793, https://doi.org/10.1029/JB078i011p01780.
[18] J. Gass, Functional Magnetic Nanoparticles, Ph.D, University of South Florida, United States – Florida, 2012.
[19] C. Scherer, A.M. Figueiredo Neto, Ferrofluids: properties and applications, Braz. J. Phys. 35 (3A) (Sep. 2005) 718–727, https://doi.org/10.1590/S0103-97332005000400018.
[20] R.E. Rosensweig, Ferrohydrodynamics, Courier Corporation, 2013.
[21] S. hwa Tan, N.-T. Nguyen, L. Yobas, T. Kang, Formation and manipulation of ferrofluid droplets at a microfluidic T-junction, J. Micromech. Microeng. 20 (Mar. 2010), 045004, https://doi.org/10.1088/0960-1317/20/4/045004.
[22] Multifunctional ferrofluid-infused surfaces with reconfigurable multiscale topography | Nature. https://www.nature.com/articles/s41586-018-0250-8.
[23] E.M. Ahmed, Hydrogel: preparation, characterization, and applications: a review, J. Adv. Res. 6 (2) (Mar. 2015) 105–121, https://doi.org/10.1016/j.jare.2013.07.006.
[24] L. Baldino, S. Cardea, E. Reverchon, Nanostructured chitosan-gelatin hybrid aerogels produced by supercritical gel drying, Polym. Eng. Sci. 58 (9) (Sep. 2018) 1494–1500, https://doi.org/10.1002/pen.24719.
[25] H. Maleki, L. Durães, A. Portugal, An overview on silica aerogels synthesis and different mechanical reinforcing strategies, J. Non-Cryst. Solids 385 (Feb. 2014) 55–74, https://doi.org/10.1016/j.jnoncrysol.2013.10.017.
[26] J.L. Gurav, I.-K. Jung, H.-H. Park, E.S. Kang, D.Y. Nadargi, Silica aerogel: synthesis and applications, J. Nanomater. 2010 (2010), 409310, https://www.hindawi.com/journals/jnm/2010/409310/. (Accessed 24 April 2020).
[27] T. Liu, M. Huang, X. Li, C. Wang, C.-X. Gui, Z.-Z. Yu, Highly compressible anisotropic graphene aerogels fabricated by directional freezing for efficient absorption of organic liquids, Carbon 100 (Apr. 2016) 456–464, https://doi.org/10.1016/j.carbon.2016.01.038.
[28] G. Chu, D. Qu, E. Zussman, Y. Xu, Ice-assisted assembly of liquid crystalline cellulose nanocrystals for preparing anisotropic aerogels with ordered structures, Chem. Mater. 29 (9) (May 2017) 3980–3988, https://doi.org/10.1021/acs.chemmater.7b00361.
[29] M. Schmidt, F. Schwertfeger, Applications for silica aerogel products, J. Non-Cryst. Solids 225 (Apr. 1998) 364–368, https://doi.org/10.1016/S0022-3093(98)00054-4.
[30] S.M. Jones, " Aerogel, Space exploration applications, J. Sol. Gel Sci. Technol. 40 (2) (Dec. 2006) 351–357, https://doi.org/10.1007/s10971-006-7762-7.
[31] G.M. Pajonk, Aerogel catalysts, Appl. Catal. 72 (2) (May 1991) 217–266, https://doi.org/10.1016/0166-9834(91)85054-Y.
[32] D.W. Cooper, Theoretical study of a new material for filters: aerogels, Part. Sci. Technol. 7 (4) (Jan. 1989) 371–380, https://doi.org/10.1080/02726358908906549.
[33] H. Tai, Z. Duan, Y. Wang, S. Wang, Y. Jiang, Paper-based sensors for gas, humidity, and strain detections: a review, ACS Appl. Mater. Interfaces 12 (28) (Jul. 2020) 31037–31053, https://doi.org/10.1021/acsami.0c06435.
[34] D. Zhang, X. Zong, Z. Wu, Y. Zhang, Hierarchical self-assembled SnS2 nanoflower/Zn2SnO4 hollow sphere nanohybrid for humidity-sensing applications, ACS Appl. Mater. Interfaces 10 (38) (Sep. 2018) 32631–32639, https://doi.org/10.1021/acsami.8b08493.
[35] C.-T. Wang, C.-L. Wu, I.-C. Chen, Y.-H. Huang, Humidity sensors based on silica nanoparticle aerogel thin films, Sensor. Actuator. B Chem. 107 (1) (May 2005) 402–410, https://doi.org/10.1016/j.snb.2004.10.034.
[36] I. Ali et al., "Humidity-responsive gold aerogel for real-time monitoring of human breath," Langmuir, vol. 34, no. 16, pp. 4908–4913, Apr. 2018, doi: 10.1021/acs.langmuir.8b00472.
[37] Ll Casas, A. Roig, E. Molins, J.m. Grenèche, J. Asenjo, J. Tejada, Iron oxide nanoparticles hosted in silica aerogels, Appl. Phys. Mater. Sci. Process 74 (5) (May 2002) 591, https://doi.org/10.1007/s003390100948.
[38] N. Shah, et al., Magnetic aerogel: an advanced material of high importance, RSC Adv. 11 (13) (2021) 7187–7204, https://doi.org/10.1039/D0RA10275J.
[39] Y. Li, et al., Programmable ultralight magnets via orientational arrangement of ferromagnetic nanoparticles within aerogel hosts, ACS Nano 13 (12) (Dec. 2019) 13875–13883, https://doi.org/10.1021/acsnano.9b04818.
[40] M. Furlan, M. Lattuada, "Fabrication of anisotropic porous silica monoliths by means of magnetically controlled phase separation in sol–gel processes, Langmuir 28 (34) (Aug. 2012) 12655–12662, https://doi.org/10.1021/la302407j.
[41] F.J. Heiligtag, M.J.I.A. Leccardi, D. Erdem, M.J. Süess, M. Niederberger, Anisotropically structured magnetic aerogel monoliths, Nanoscale 6 (21) (Oct. 2014) 13213–13221, https://doi.org/10.1039/C4NR04694C.
[42] N. Leventis, I.A. Elder, G.J. Long, D.R. Rolison, Using nanoscopic hosts, magnetic guests, and field alignment to create anisotropic composite gels and aerogels, Nano Lett. 2 (1) (Jan. 2002) 63–67, https://doi.org/10.1021/nl015637a.
[43] B. Wang, A. Reifsnyder, I. Zharov, and K. Carlson, "Silica aerogel membranes fabricated using removable nitrocellulose scaffolds," Microporous Mesoporous Mater., vol. 278, pp. 435–442, Apr. 2019, doi: 10.1016/j.micromeso.2018.12.045.
[44] I. Nelson, et al., Freeze-casting of surface-magnetized iron(II,III) oxide particles in a uniform static magnetic field generated by a Helmholtz coil, Adv. Eng. Mater. 21 (3) (2019) 1801092, https://doi.org/10.1002/adem.201801092.
[45] M. R. Miner, B. Hosticka, and P. M. Norris, The Effects of Ambient Humidity on the Mechanical Properties and Surface Chemistry of Hygroscopic Silica Aerogel.
[46] R.J. Hunter, Foundations of Colloid Science, Clarendon Press, 1987.